

Dual stage and an image processing-based method for sight stabilization[†]

Joon Lyou^{1,*}, MinSig Kang², HwyKuen Kwak¹ and YoungJun Choi³

¹Department of Electronics Engineering, Chungnam National University, Daejeon, 305-764, Korea

²Department of Mechanical Engineering, Kyungwon University, Sungnam, Kyunggi-Do, 461-701, Korea

³Agency for Defense Development, Yuseong P.O Box 35, Daejeon, 305-600, Korea

(Manuscript Received June 17, 2008; Revised January 20, 2009; Accepted March 9, 2009)

Abstract

This paper presents a combined dual stage-based mechanical and image-based stabilization scheme for a three-axis image-tracking sight system. To improve the stabilization and tracking accuracy, a secondary stage actuated by a pair of electro-magnets is mounted on a conventional elevation gimbal. For the remaining roll axis stabilization, an electronic digital- image stabilization technique is introduced to estimate and correct roll motions. Experimental results are given to demonstrate the effectiveness of the proposed stabilization system and the image-stabilization scheme.

Keywords: Sight stabilization; Dual stage; Image processing; Electro-magnets; Rotated image

1. Introduction

Target image-tracking sight systems mounted on moving vehicles such as main battle tanks and armored vehicles, require high stabilization characteristics. This implies maintaining the line of sight accurately on the selected object when the vehicles are stationary or when they are moving. Major stabilization error sources include the engine, the cooling fan, and irregular terrains. Although three-axis stabilization is necessary to gain perfect stabilization of a target image, in conventional sight systems, two-axis gimbal-structured mechanical stabilization is adopted because three-axis mechanical stabilization is exceedingly bulky and expensive. However, modern fire control systems require three-axis stabilization performance including the pitch, yaw, roll axes for long-range observation and higher accuracy.

In this paper, a combined dual-stage-based servo mechanism and digital-image-based stabilization scheme are suggested to improve the stabilization

performance without an increase of the volume. This will allow it to be added to the conventional two-axis stabilization system.

Dual-stage structured servo-systems have been used for fast tool servos capable of generating fast but small range tool motion for precision machining [1, 2]. Also, dual-stage actuation has been suggested by many as the solution for high density hard disk drives. In a typical proposed dual-stage HDD, a small secondary actuator by means of PZT micro-actuator is appended on the voice coil motor for fine positioning [3]. The main purposes of dual-stage actuation are increasing servo-bandwidth and positioning accuracy.

Recently, a dual-stage servo mechanism has been developed for an image-tracking system to improve transient control measures such as the small rise time, small overshooting, and the small settling time [4]. A secondary stage, a platform actuated by a pair of electro-magnets, mounted on a conventional elevation gimbal. In this mechanism, the gimbal provides a large rotation range but slow motion, and the platform provides a small rotation range but fast positioning. Apart from dual-stage systems used in fast tool servos and in hard disk drives, the first stage, the gimbal, and the second stage, the platform, are dynamically cou-

[†] This paper was recommended for publication in revised form by Associate Editor Dong Hwan Kim

* Corresponding author. Tel.: +82 42 8215669, Fax.: +82 42 8235436

E-mail address: jlyou@cnu.ac.kr

© KSME & Springer 2009

pled each other apparently because the platform is hinged on the gimbal.

As the dual-stage servo mechanism exhibits dynamic coupling, a sliding mode control is applied to the platform positioning system to attain robust performances and stability in the presence of the disturbances related to the gimbal motion.

Sliding mode control is widely used in control of uncertain systems, mainly due to its robust characteristics with respect to parameter uncertainties and external disturbances. Various methods based on sliding mode control framework have been applied to precision motion control systems in the consideration of model uncertainties and disturbances.

In this paper, to apply a sliding mode control, system parameter uncertainties caused from linearization of electro-magnetic actuating force were analyzed to establish reachability to sliding surface. The effectiveness of the sliding mode control was verified along with some experimental results.

Instead of adding a new mechanical gimbal to stabilize the image in the roll direction, a digital-image-based roll motion estimation and correction algorithm is devised. To be specific, an equivalent rotation model that accounts for the combined motion of rotation and translation is derived. Based on the model, the rotation center and angle are estimated, and motion compensation is then achieved. The estimation algorithm computes the rotational center from selected local motion vectors of related pixels using least square methods, and the rotational angle is determined from a special subset of motion vectors. To offset the motion, two algorithms are used: frame-to-frame and frame-to-reference [5]. Motion compensation is performed essentially by nearest-neighbor interpolation. Here, the present estimation algorithm does not require a time-consuming parameter search. The frame-to-reference algorithm was implemented on DSP TMS320DM642, and it was confirmed to runs at the rate of 16 frames per second.

The proposed stabilization mechanism and the image-stabilization scheme were applied to an experimental set-up. Various experimental results are illustrated below.

2. Sight stabilization system

The overall structure and signal flow of the stabilization system are illustrated in Fig. 1. The dual-stage-based mechanical stabilization part and the electronic

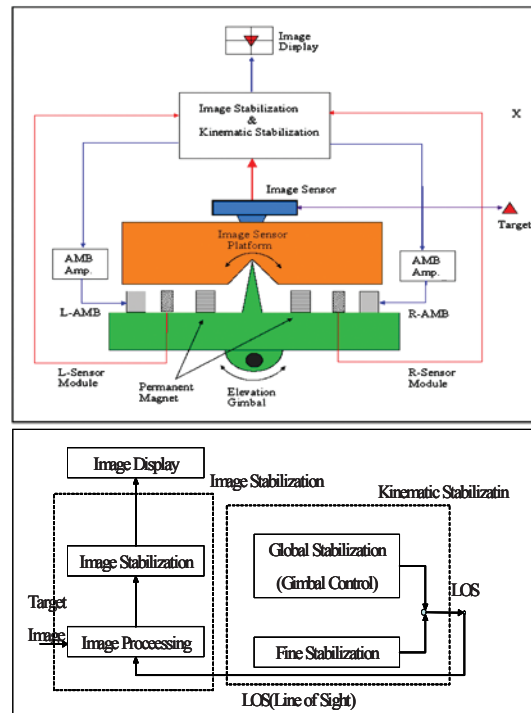


Fig. 1. Flowchart for combined LOS stabilization system.

digital image stabilization part complement each other to minimize the line of sight stabilization errors of the sight system. Actually, elevation(pitch) and azimuth(yaw) stabilization errors are mainly diminished by the dual servomechanism, while rotation(roll) errors are stabilized by the digital image processing.

2.1 Dual stage mechanical stabilization

2.1.1 Dynamic equation

In consideration of the performance limitations of the conventional gimbal structured stabilization system, a dual-stage servo-system was adopted. In the dual-stage servo-mechanism, a platform is mounted on an existing motor-driven gimbal. The gimbal rotates by a wide range, but is susceptible to friction and has large reaction time. On the other hand, the platform which is actuated by a pair of electro-magnets rotates in a small range, has small reaction time. Moreover, the platform is only slightly influenced by friction because it is supported by a sharp edge at its center. The electro-magnetically controlled platform system also provides advantages such as good linearity, excellent responsiveness, and high accuracy. Taking advantages of each stage, the dual stage can

improve the stabilization performance over a wide rotation range.

The dynamic model of the dual-stage system in Fig. 2 can be represented as (1).

$$\begin{aligned} J_b \ddot{\phi}_b + B_b \dot{\phi}_b &= -T_p + T_m + T_d \\ J_p (\ddot{\phi}_p + \ddot{\phi}_b) + B_p \dot{\phi}_p &= T_p \\ T_p &= F_c L, T_m = K_m i_m \end{aligned} \tag{1}$$

where ϕ_b and ϕ_p represent the rotation angle of the gimbal and the platform rotation angle with respect to the gimbal, respectively. J_b and B_b are the mass moment of inertia and the rotational viscous friction coefficient of the gimbal, respectively. J_p and B_p denote the mass moment of inertia and the rotation viscous frictional coefficient of the platform, respectively. T_m is the motor torque driving the gimbal, and T_p is the torque generated by the electro-magnetic actuator. K_m is the torque constant of the gimbal driving motor and i_m is the motor current, respectively. L is the distance between rotation axis of the gimbal and the electro-magnetic actuator position, and F_c denotes the electro-magnetic force. The attractive force by a pair of electro-magnetic actuators can be represented as

$$F_c = \frac{\mu_0 N^2 A}{4} \left[\left(\frac{I_0 + i}{y_0 - y} \right)^2 - \left(\frac{I_0 - i}{y_0 - y} \right)^2 \right] \tag{2}$$

The attractive force in (2) can be linear about the operating position if the deviation of the air-gap y is small enough relative to the standard air-gap (y_0), and if the control current i is small enough compared to the bias current (I_0) as follows.

$$F_c = K_y y + K_c i \tag{3}$$

Here F_c is the electromagnetic force and K_y and K_c are the position stiffness and the current stiffness coefficients, respectively.

From (1) and (3), the equation of motion of the platform can be written as

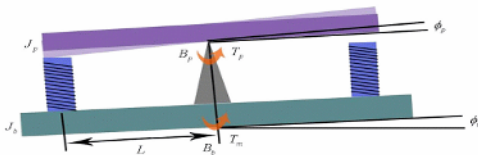


Fig. 2. Dual-stage system.

$$\begin{aligned} J_b \ddot{\phi}_b + B_b \dot{\phi}_b &= -K_y L^2 \phi_p - K_c L i_c + K_m i_m + T_d \\ J_p \ddot{\phi}_p + B_p \dot{\phi}_p - K_y L^2 \phi_p &= K_c L i_c - J_p \ddot{\phi}_b \end{aligned} \tag{4}$$

As the stiffness of the platform dynamic model is negative in (4), this system is inherently unstable.

From (4), the dynamic model of the dual-stage system can be rewritten as given in (5).

$$\begin{aligned} \Phi_p(s) &= G_M(s)(I_c(s) + \Delta_1) \\ \Phi_b(s) &= G_F(s)(I_m(s) + \Delta_2) \end{aligned} \tag{5}$$

where

$$\begin{aligned} G_M(s) &= \frac{K_c L}{J_p s^2 + B_p s - K_y L^2}, G_F(s) = \frac{K_m}{J_b s^2 + B_b s} \\ \Delta_1 &= -\frac{J_p s^2}{K_c L} \Phi_b(s) \\ \Delta_2 &= -\frac{K_y L^2}{K_m} \Phi_p(s) - \frac{K_c L}{K_m} I_c(s) + \frac{1}{K_m} T_d(s) \end{aligned}$$

2.1.2 Dual-stage control

As can be seen in (5), the angular acceleration of the gimbal excites the platform. Clearly, this coupled dynamics can increase the complexity in the design of the controller. In this paper, a sliding mode control is applied to decouple the platform dynamics from the gimbal dynamics and attain robust control performance. Fig. 3 shows the application of a sliding mode control for the dual-stage system. K_M and K_F are the controllers for the platform and the gimbal, respectively. As can be seen in Fig. 3, the gimbal control is designed to track the given reference position r and the platform control is designed to compensate the tracking error of the gimbal such that the absolute position of the platform tracks the reference position input.

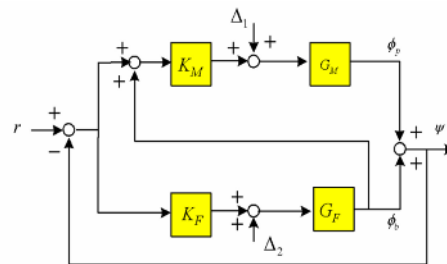


Fig. 3. Sliding mode control of the dual-stage system.

The tracking error can be written as

$$E(s) = \frac{R(s)}{(1 + K_M G_M)(1 + K_F G_F) - \frac{G_M \Delta_1 + G_F(1 + K_M G_M) \Delta_2}{(1 + K_M G_M)(1 + K_F G_F)}} \quad (6)$$

To design the platform controller in the form of a sliding mode control, a sliding surface σ_p is defined as follows:

$$\sigma_p = S_p x_p \quad (7)$$

where $S_p \in R^{*l}$ is a vector to define the sliding surface and x_p is an augmented state vector defined by

$$x_p = [\int e_p dt \quad e_p \quad \dot{e}_p]^T, \quad e = r - \phi_b - \phi_p.$$

The control input of the sliding mode control sums both the equilibrium control input u_{eq} and the reaching control input u_{np} .

$$u_p(t) = u_{eq}(t) + u_{np}(t) \quad (8)$$

It is straightforward to derive the equilibrium control input and the reaching control input according to the standard sliding mode control design technique.

2.2 Image-based stabilization

A digital-image stabilization system essentially consists of two main processes: one for motion estimation and the other for motion compensation. Motion estimation can be divided into local motion estimation and global motion estimation. Local motion is the movement of individual image pixels between two consecutive image frames. From the local motion vectors, global motion estimation can be computed using a motion model. Motion compensation is the process of removing unwanted motion using global motion estimation. Fig. 4 shows the configuration of a general DIS system.

2.2.1 Local motion estimation

Local motion is the movement of individual image pixels between two consecutive image frames. It can be obtained by block matching, an optical flow technique, or tracking predetermined dominant features.

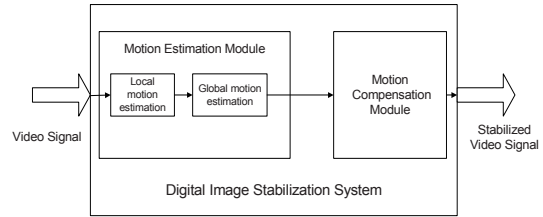


Fig. 4. Digital image stabilization process.

Block matching can be considered as the most popular method for practical local motion estimation as it has less hardware complexity. As a result, it is widely available in VLSI. Moreover, nearly all H.262 MPEG codecs utilize block matching for motion estimation. As the most popular choice for the practical implementations is MAD, it is used as the criterion for the local motion estimation [6].

$$MAD(d_1, d_2) = \frac{1}{N_1 N_2} \sum_{(x,y) \in B} |s(x, y, k) - s(x + d_1, y + d_2, k + 1)| \quad (9)$$

Here B denotes an $N_1 \times N_2$ block for a set of candidate motion vectors (d_1, d_2) . The estimation of the motion vector is given the value of (d_1, d_2) which minimizes the MAD value. That is expressed as,

$$[d_1, d_2]^T = \arg \min_{(d_1, d_2)} MAD(d_1, d_2) \quad (10)$$

The output of block matching is the local motion vector field $V(x, y) = (u(x, y), v(x, y))$ of each block at (x, y) . For a practical case, the motion vectors from actual images are usually corrupted by the noise in the images. To reduce motion noise, a median filter is applied to the local motion fields.

2.2.2 Global motion estimation

From the local motion vectors, the global motion can be estimated by a motion model. When a consecutive image sequence is rotated purely at arbitrary rotational center (x_0, y_0) at rotational angle θ , the movement of a pixel point between image frames behaves as shown in Fig. 5.

For translational motion combined with pure rotational motion, it is possible to express the relationship between pixel movements as follows:

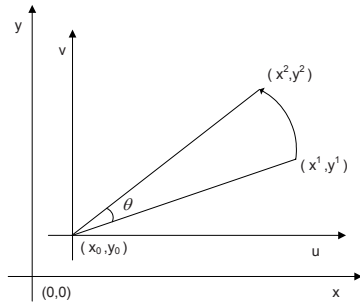


Fig. 5. Movement of pixel point after pure rotational motion.

$$\begin{bmatrix} x^2 \\ y^2 \end{bmatrix} = \begin{bmatrix} \cos \theta & -\sin \theta \\ \sin \theta & \cos \theta \end{bmatrix} \begin{bmatrix} x^1 - x_0 \\ y^1 - y_0 \end{bmatrix} + \begin{bmatrix} x_0 \\ y_0 \end{bmatrix} + \begin{bmatrix} d_x \\ d_y \end{bmatrix} \tag{11}$$

Here d_x and d_y are translational movements in the x and y directions between frames respectively. The point (x^1, y^1) is the pixel of the first image frame, the point (x^2, y^2) is that of the second image frame.

Using (11) for all N -matched point pairs of local motion between image frames, results in a system of $2N$ linear equations in five unknowns (θ, x_0, y_0, d_x and d_y). Rearranging (11) in the matrix for $b=Ax$, gives

$$\begin{bmatrix} x_1^2 - x_1^1 \\ x_2^2 - x_2^1 \\ \vdots \\ x_N^2 - x_N^1 \\ y_1^2 - y_1^1 \\ y_2^2 - y_2^1 \\ \vdots \\ y_N^2 - y_N^1 \end{bmatrix} = \begin{bmatrix} -y_1^1 & 0 & 1 & 1 & 0 \\ -y_2^1 & 0 & 1 & 1 & 0 \\ \vdots & \vdots & \vdots & \vdots & \vdots \\ -y_N^1 & 0 & 1 & 1 & 0 \\ x_1^1 & -1 & 0 & 0 & 1 \\ x_2^1 & -1 & 0 & 0 & 1 \\ \vdots & \vdots & \vdots & \vdots & \vdots \\ x_N^1 & -1 & 0 & 0 & 1 \end{bmatrix} \begin{bmatrix} \theta \\ K \\ L \\ d_x \\ d_y \end{bmatrix}, \quad \bar{b} = \bar{A}x \tag{12}$$

where K and L are substituted for $x_0\theta$ and $y_0\theta$ in (12).

As the rank of matrix A is three, it is not possible to obtain directly unique five unknowns from (12). To estimate the five parameters, more information between consecutive frames is needed or another approach must be used. Chang [8] proposed digital image translational and rotational motion stabilization based on searching method. He first estimated the rotational center using a search method and then obtained translational motions. However, this method has several restrictions in terms of implementation. It

involves a time-consuming process as it determines the rotational center on a searching basis. Moreover, whole image pixels must be searched to locate the rotational center of the first image frame, as the searching area is determined by the estimated rotational center of the previous frame. Additionally, if the estimated rotational center of present frame is not in the searching area due to noise, the estimation error will be increased considerably from the next frame.

In the proposed method, the estimation method is considered depending only on a single rotation model that can accommodate the combined motion of rotation and translation instead of computing as estimation of the rotational and translational motion parameters.

The model equation for estimation of both the rotational and translational motion is given by (13). Likewise, a basic rotation model is defined as

$$\begin{bmatrix} x^2 \\ y^2 \end{bmatrix} = \begin{bmatrix} \cos \theta & -\sin \theta \\ \sin \theta & \cos \theta \end{bmatrix} \begin{bmatrix} x^1 - \alpha \\ y^1 - \beta \end{bmatrix} + \begin{bmatrix} \alpha \\ \beta \end{bmatrix} \tag{13}$$

From (12) and (13), α and β are obtained such that

$$\alpha = \{ (1 - \cos \theta)(-\cos \theta \cdot x_0 + \sin \theta \cdot y_0 + x_0 + d_x) + \sin \theta(\sin \theta \cdot x_0 + \cos \theta \cdot y_0 - y_0 - d_y) \} / \{ 2(1 - \cos \theta) \} \tag{14-1}$$

$$\beta = \frac{1}{1 - \cos \theta} [-\sin \theta \cdot x_0 - \cos \theta \cdot y_0 + y_0 + d_y + \sin \theta \{ (1 - \cos \theta)(-\cos \theta \cdot x_0 + \sin \theta \cdot y_0 + x_0 + d_x) + \sin \theta(\sin \theta \cdot x_0 + \cos \theta \cdot y_0 - y_0 - d_y) \} / 2(1 - \cos \theta)] \tag{14-2}$$

where $\theta \neq n \cdot \pi$ (n is integer).

According to (13) and (14), it follows that the model of both rotational and translational motion can be expressed by the single rotation model, and that the global motion estimation is actually serves to determine the rotation model parameters of (11), that is, the rotation center and angle.

The block motion and median filtering result is the local motion vectors of each pixel in the current image frame. The local motion vectors at any point (x, y) are expressed as

$$u = x^2 - x^1, v = y^2 - y^1 \tag{15}$$

where point (x^2, y^2) in the second image frame is matched with point (x^1, y^1) in the first frame after pure

rotation, and u, v are each components of the motion vector for the x -axis and the y -axis. For the case of pure rotational motion, the motion vectors at any points coincide with the tangential line of the circle, which has a center point identical to the image rotational center. Therefore, all of the perpendicular lines against motion vectors in any arbitrary points cross at one point, the rotational center, as described in Fig. 6.

The perpendicular line at half of the local motion vector of the points $A_1(x_1, y_1)$ and $A_2(x_2, y_2)$ can be represented by (16) & (17), respectively. For A_1 ,

$$y = a_1x + b_1 \tag{16}$$

where $a_1 = -u_1/v_1$, $b_1 = (y_1 + v_1/2) - a_1(x_1 + u_1/2)$, and u_1, v_1 are the local motion vectors at A_1 .

For the point A_2 ,

$$y = a_2x + b_2 \tag{17}$$

where $a_2 = -u_2/v_2$, $b_2 = (y_2 + v_2/2) - a_2(x_2 + u_2/2)$ and u_2, v_2 are the local motion vectors at A_2 .

Although two distinct points are sufficient for the computation of the rotation center, noises and insufficient image contrast often cause erroneous results. To guarantee the robustness of the computed results under a noisy environment, over-determined systems are utilized that involve more than three equations.

For the case of N points, N equations are obtained.

$$\begin{bmatrix} -a_1 & -a_2 & \dots & -a_N \\ 1 & 1 & \dots & 1 \end{bmatrix}^T \begin{bmatrix} x_0 \\ y_0 \end{bmatrix} = [b_1 \quad b_2 \quad \dots \quad b_N]^T \tag{18}$$

This can be rewritten in matrix vector form, as

$$Ax = b \tag{19}$$

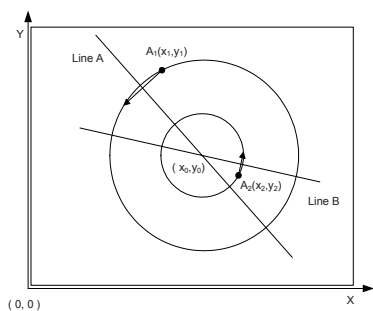


Fig. 6. Rotation center estimation.

The rotation center is then obtained by

$$x = (A^T A)^{-1} A^T b \tag{20}$$

After finding the rotation center, the rotation angle θ can be computed from the law of trigonometry, as depicted in Fig. 7.

The point (x_0, y_0) is the estimated rotational center. By matching (x^2, y^2) in the second image frame with (x^1, y^1) in the first frame after a motion, the rotation angle is obtained.

$$\theta = \tan^{-1} \frac{(y^2 - y_0)(x^1 - x_0) - (x^2 - x_0)(y^1 - y_0)}{(x^2 - x_0)(x^1 - x_0) + (y^2 - y_0)(y^1 - y_0)} \tag{21}$$

Considering the numerical reliability, the mean of the estimated values at N matched points is also utilized.

2.2.3 Motion compensation

Motion compensation is the process of removing unwanted motion by using the global motion estimation. Two possible implementations are considered: the first always uses two consecutive frames from the input image sequence to estimate the motion parameters; it is known as the frame-to-frame algorithm(FFA). The second keeps some reference image and uses it to estimate the motion between the reference and the current input image; it is known as the frame-to-reference algorithm(FRA) [9].

Prior to the motion correction, a source coordination of the pixel is done by using the rotation center and angle as follows:

$$\begin{bmatrix} x' \\ y' \end{bmatrix} = \begin{bmatrix} \cos \theta & -\sin \theta \\ \sin \theta & \cos \theta \end{bmatrix}^{-1} \begin{bmatrix} x - x_c \\ y - y_c \end{bmatrix} + \begin{bmatrix} x_c \\ y_c \end{bmatrix} \tag{22}$$

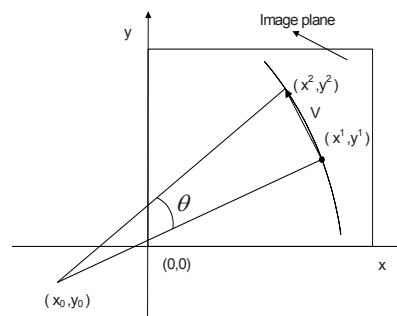


Fig. 7. Rotation angle estimation.

Here (x_c, y_c) is the center of the rotation, (x, y) is the position after rotation, and (x', y') denotes the position before rotation. Motion compensation is then performed by nearest-neighbor interpolation.

$$f(x, y) = f(f_{rnd}(x'), f_{rnd}(y')) \quad (23)$$

Here, $f(x, y)$ is the gray level at the pixel position (x, y) , and $f_{rnd}(x)$ is the rounding operation that converts the floating number x to an integer.

For real-time implementation, a recursive version of FRA is derived as follows. It is possible to express the relationship between the 1st and the k th images frame as

$$\begin{aligned} \begin{bmatrix} x_1 \\ y_1 \end{bmatrix} &= \mathfrak{R}_2 \mathfrak{R}_3 \cdots \mathfrak{R}_{k-1} \mathfrak{R}_k \begin{bmatrix} x_k \\ y_k \end{bmatrix} + \mathfrak{R}_2 \mathfrak{R}_3 \cdots \mathfrak{R}_{k-1} \begin{bmatrix} K_{k-1} \\ L_{k-1} \end{bmatrix} \\ &+ \mathfrak{R}_2 \mathfrak{R}_3 \cdots \mathfrak{R}_{k-2} \begin{bmatrix} K_{k-2} \\ L_{k-2} \end{bmatrix} + \cdots + \mathfrak{R}_2 \begin{bmatrix} K_3 \\ L_3 \end{bmatrix} + \begin{bmatrix} K_2 \\ L_2 \end{bmatrix} \end{aligned} \quad (24)$$

That is,

$$\begin{bmatrix} x_1 \\ y_1 \end{bmatrix} = \mathfrak{R}_2^{k-1} \mathfrak{R}_k \begin{bmatrix} x_k \\ y_k \end{bmatrix} + \mathfrak{R}_2^{k-1} \begin{bmatrix} K_{k-1} \\ L_{k-1} \end{bmatrix} + S_{k-1} \quad (25)$$

where

$$\mathfrak{R}_k = \begin{bmatrix} \cos \theta_k & -\sin \theta_k \\ \sin \theta_k & \cos \theta_k \end{bmatrix}, \begin{bmatrix} K_k \\ L_k \end{bmatrix} = -\mathfrak{R}_k \begin{bmatrix} x_{ck} \\ y_{ck} \end{bmatrix} + \begin{bmatrix} x_{ck} \\ y_{ck} \end{bmatrix} \quad (26)$$

and $R_2^{k-1} = R_2 R_3 \cdots R_{k-1}$ and S_{k-1} represent the remaining terms on the right side of (24). In (25), R_2^{k-1} and S_{k-1} can be calculated at the $(k-1)$ th image frame. This recursive nature does not increase the amount of computation for each frame.

3. Experiment results

An experimental set-up for dual-stage and image-based line-of-sight stabilization system is shown in Fig. 8. The experimental set-up consists of a dual-stage mechanism, a platform on a gimbal, a pan-tilt driving mechanism on the platform, and a camera on the platform for image acquisition. Even though actual sight system has two rotation axes, pitch and yaw axes, as a preliminary study, the dual-stage mechanism in the experimental set-up is constrained

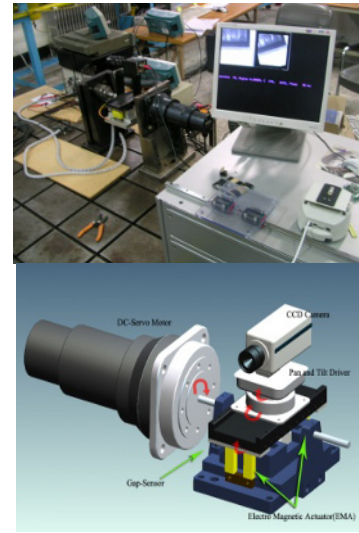


Fig. 8. Stabilization device for roll-axis compensation.

to rotate only in the pitching direction. It may straightforward to apply the controls developed for the pitch direction to the yaw direction. The pan-tilt driving system generates roll motion of the camera to simulate roll motion of vehicle moving on a typical terrain.

Some experiments were carried out in order to evaluate the stabilization performance of the dual-stage and image-based stabilization complex system. In detail, pitch-axis stabilization was performed by the dual-stage scheme and roll-axis stabilization by the image-based scheme.

Fig. 9(a) and (b) show independent step responses of the gimbal and the platform, respectively. The rise times of the platform and the gimbal are determined to be 0.04s and 0.5s, respectively. Obviously, the platform dynamics is much faster than the gimbal dynamics. This implies the dual-stage mechanism can improve stabilization performance sufficiently compared to the gimbal-structured stabilization system. As far as mechanical resonance does not occur, the gain of the gimbal controller was designed to be as high as possible.

A typical step response of the dual-stage given in Fig. 9(c) illustrates advantages of the dual-stage mechanism compared to conventional gimbal systems. As expected from Fig. 9(a) and (b), the platform reaches to the desired position very quickly; meanwhile the gimbal almost starts to move, and as the gimbal reaches the desired position slowly the platform return to its nominal position along almost

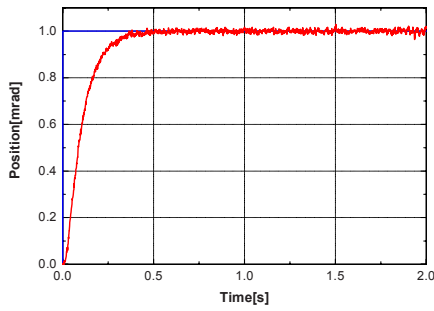


Fig. 9(a). Step response of gimbal.

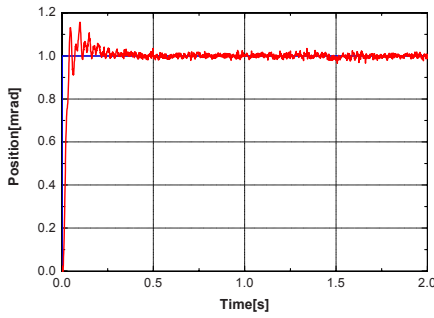


Fig. 9(b). Step response of platform.

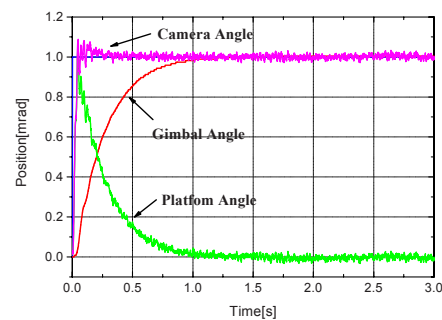


Fig. 9(c). Step response of dual-stage.

reverse motion profile of the gimbal so that the camera aims the reference position within 0.04s and maintained at the desired position. In all experiments, the sampling frequency was kept as 10 KHz.

To demonstrate the effectiveness of the proposed digital image stabilization algorithm, simulation results were illustrated for synthetic images. Additionally, to show the possibility of an actual system application, hardware implementation results on real images are described. The fidelity of an image-stabilization technique is evaluated by the peak signal-to-noise ratio (PSNR) between stabilized frames [5]. The PSNR between consecutive frame I_1 and I_0 is defined as

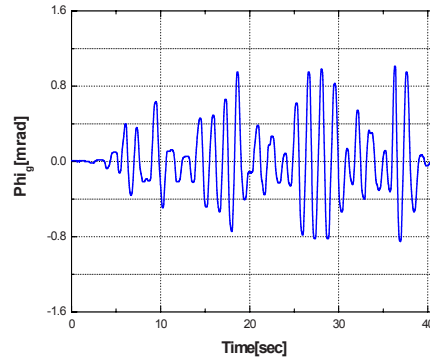


Fig. 10. The base disturbance of gimbal system.

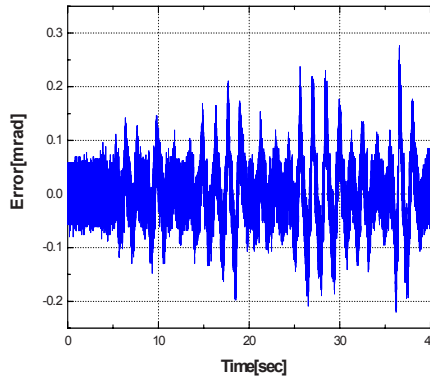


Fig. 11. Error response of dual stage system.

$$PSNR(I_1, I_0) = 10 \log \frac{255^2}{MSE(I_1, I_0)} \quad (27)$$

where the mean squared error (MSE) is a measure of the average departure per pixel from the desired stabilized result.

In this experiment, pitch-axis stabilization error of a sight system is generated by the gimbal and roll-axis stabilization error is generated via pan-tilt, simultaneously. The stabilization error in the pitch-direction is stabilized by the platform and roll-direction error is compensated by the image-based stabilization.

The rotation angle of the gimbal which simulates disturbance motion of a vehicle moving on a typical terrain is shown in Fig. 10. Under this disturbance, the stabilization error compensated by the platform is shown in Fig. 11. The standard deviation of stabilization error σ is determined to be 0.0613mrad.

Fig. 12 shows the image with error along with the offset image. The DIS part shows the same result as the compensation for roll-axis stabilization, as pitch-axis stabilization is offset by the kinematics

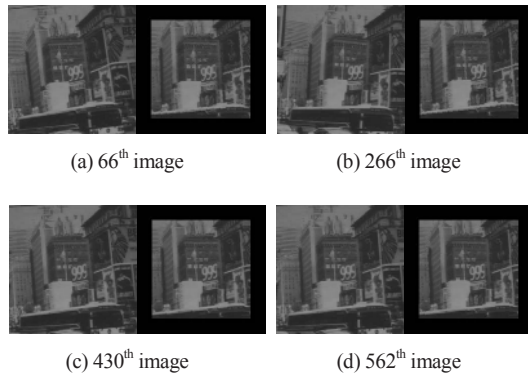


Fig. 12. Result images for roll-axis compensation.

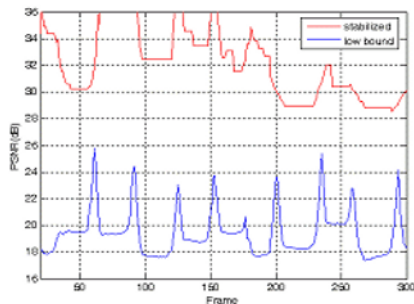


Fig. 13. PSNR for the roll axis compensation.

stabilization part. The experiment was performed for 600 frames in order to set the kinematics stabilization part to the time. Fig. 13 shows the PSNR, showing that image stabilization was successful.

This experimental result can be evaluated for two-axis stabilization application prospects through pitch stabilization by a mechanical device and roll stabilization by image processing. In addition, the sight system of three-axis stabilization may be evaluated because yaw stabilization can be included in the manner of pitch stabilization.

4. Conclusion

A combined kinematic and image-based scheme for three-dimensional line of sight stabilization system is proposed. To verify its effectiveness, the proposed scheme was implemented on an experimental set-up. From the experimental results, it was confirmed that a dual-stage servo mechanism controlled by a sliding mode control is effective to attain a wider range of rotation with high accuracy and rapid responses. Moreover, it was found that the digital-image based roll motion estimation and compensation

scheme can improve stabilization performance without the addition of a new mechanical roll gimbal. These results are likely applicable to sight systems on the moving vehicles and platforms.

Acknowledgment

This work was supported by grant No. R01-2003-000-10857-0 from the Basic Research Program of the Korea Science Engineering Foundation.

References

- [1] K. Krishnamoorthy, C. Y. Lin and T. C. Tsao, Design and control of a dual-stage fast tool servo for precision machining, *Proc. of the 2004 IEEE International Conference on Control Applications*, (2004) 742-747.
- [2] B. S. Kim and T. C. Tsao, Control of a dual-stage actuator system for noncircular cam turning process, *Proc. of the American Control Conference*, Arlington, VA, (2001) 25-27.
- [3] M. Kobayashi and R. Horowitz, Tracking seek control for hard disk dual-stage servo systems, *IEEE Trans. Magnetics*, 37 (2) (2001) 949-954.
- [4] M. Young, *The Technical Writer's Handbook*, Mill Valley, CA: University Science (1989).
- [5] C. Morimoto and R. Cellappa, Evaluation of image stabilization algorithms, *Proc. of IEEE Conference on Acoustics, Speech and Signal Processing*, 5 (1999) 2789-2792.
- [6] A. M. Tekalp, *Digital Video Processing*, Prentice-Hall, USA, (1995).
- [7] K. Uomori, A. Morimura and H. Ishii, Electronic image stabilization system for video cameras and VCRs, *Journal of the Society of Motion Picture Television Engineers*, 101 (1992) 66-75.
- [8] J. Y. Chang, W. F. Hu, M. H. Cheng and G. S. Chang, Digital image translational and rotational motion stabilization using optical flow technique, *IEEE Transactions on Consumer Electronics*, 48(1) (2002) 108-115.
- [9] C. Morimoto and R. Chellappa, Fast electronic digital image stabilization for off-road navigation, *Real-Time Imaging*, 2 (1996) 285-296.
- [10] Y. P. Park and H. S. Yang, Technology trends for high recording density in HDD, *Journal of the Korean Society of Precision Engineering*, 18(4) (2001) 9-19.



Joon Lyou received a B.S. degree in Electronics Engineering from Seoul National University in 1978. He then went on to receive M.S. and Ph.D. degrees from KAIST in 1980 and 1984, respectively. Dr.

Lyou is currently a professor of the Department of Electronics Engineering at Chungnam National University in Daejeon, Korea. His research interests include industrial control and sensor signal processing, IT based robotics, and navigation systems.



MinSig Kang received a B.S. degree from the Department of Mechanical Engineering of Seoul National University in 1980. He then went on to receive M.S. and Ph.D. degrees from KAIST in 1983 and 1987, respectively. He worked for the

Agency for Defence Development during 1987-1998. Dr. Kang is currently a professor of the Department of Mechanical and Automotive Engineering at Kyungwon University in Sunnam, Korea. His research interests include dynamic systems measurement and control, industrial robotics, and manufacturing systems.



HwYKuen Kwak received a B.S. degree in Electronics Engineering from Chungnam National University in 2005. He is currently working on his M.S. and Ph.D. course at Chungnam National University in Daejeon, Korea. His research areas are

image signal processing, sensors and digital control systems.



YoungJun Choi received a B.S. and M.S. degree in Mechanical Engineering from Kyungwon University in 2004 and 2006. He is currently a researcher for the Agency for Defence Development in Daejeon, Korea. His research fields are dynamic

systems measurement and control, satellite systems, navigation systems and smart materials.